Insight into the oxidation mechanism of furanic compounds on Pt(111)

Lesli O. Mark[1], Naveen Agrawal[2], Alex M. Román[1], Adam Holewinski[1], Michael J. Janik[2], and J. Will Medlin[1]

[1]University of Colorado, Boulder, Department of Chemical and Biological Engineering, Boulder, CO 80303

[2]Pennsylvania State University, Department of Chemical Engineering, University Park, PA 16802

Keywords: direct oxidation, platinum, furan, furfuryl alcohol, oxygen covered surface, vibrational spectroscopy

Abstract

Partial oxidation of multifunctional oxygenates is of interest for the production of high-value chemicals, but the understanding of the mechanism on Pt catalysts is lacking. To probe the effects of oxygen in the reaction of furanics on Pt(111), temperature-programmed desorption (TPD), high-resolution electron energy loss spectroscopy (HREELS), electrochemical catalytic experiments, and density functional theory (DFT) calculations were conducted. The presence of oxygen on the Pt(111) surface significantly altered the reaction paths for furan and furfuryl alcohol oxidation.

Whereas furan desorbed without reaction from clean Pt(111) during TPD, on the O pre-covered surface extensive oxidation and decomposition reactions were observed. The main volatile products were H_2O, CO, and CO_2. HREEL spectra and DFT calculations indicated that furan initially reacted through oxygen addition to the ring to produce surface adsorbed furanone intermediates. For furfuryl alcohol, the same desorption products were formed, but maleic anhydride (MA) was also detected as a trace product. HREELS and DFT calculations suggested that alcohol oxidation proceeded through dehydrogenation at the hydroxyl and methylene groups and subsequent oxidation to produce a carboxylate intermediate. The carboxylate intermediate underwent decarboxylation to form CO_2 and surface furyl intermediates, which then underwent deep oxidation and decomposition. Thus, the presence of the oxygenated side chain on the furan ring for furfuryl alcohol strongly influenced the oxidation chemistry. Comparison of furfural electrocatalytic oxidation results on Pd (collected here) and Pt (from previous work) indicated that Pt is less active for C-C activation but more active for insertion of oxygen atoms into the furan ring, in line with the current and previously published surface science results.

Introduction

Integrated biorefineries rely on the production of value-added chemicals through the oxidation of biomass-derived products [1,2]. Of the variety of biomass-derived compounds, furanics such as furan, furfural, and furfuryl alcohol have been of interest because they are useful as platform compounds to derive industrially applicable chemicals and biofuels [3–5]. The valorization of such compounds often involves separation processes followed by energy intensive thermochemical processing, but aqueous phase thermo-catalytic and electro-catalytic methods have received attention for economically viable oxidation of furanic molecules [6]. Thermochemically, 5-

hydroxymethylfurfural oxidation has been shown to be active on Pd/C catalysts to form 2,5-furan dicarboxylic acid [7] and Pd(111) has been shown to oxidize primary alcohols, furanic, and benzylic compounds [8–10]. Electrocatalytic systems have shown successful oxidation of HMF to furandicarboxylic acid (FDCA) [11–17]. These thermochemical and electrocatalytic systems, often in aqueous environments, complicate efforts to probe surface-adsorbate interactions, and can introduce surface adsorbed O or OH species to participate in reactions[18,19]. Understanding the role of surface adsorbed oxygen in facilitating or directing furanic species oxidation can aid in selective catalyst design [9].

Reactions of furan, furfural, and furfuryl alcohol have been studied extensively on clean metal surfaces; these studies indicate a significant dependence of product selectivities and kinetics on surface composition[20–24]. There have also been several surface-level studies of the effect of adsorbed oxygen on the reactions of complex alcohol and furanic species on Pd(111). Furfuryl alcohol was found to undergo dehydrogenation to furfural, which reacted with surface oxygen to produce an adsorbed furoate (C_4H_3OCOO*) that decarboxylated to produce furan and CO_2[9]. Furan reacted with surface oxygen to produce partial oxidation products 2(5H)-furanone (25HF) and maleic anhydride (MA)[9]. Similar results were seen for benzyl alcohol on oxygen-precovered Pd(111)[10]. Although oxidation of furanic species has not to our knowledge been studied on Pt(111), methanol oxidation was found to proceed through the formation of an adsorbed formate intermediate on Pt(111) [25]. Another relevant study of furan was on oxygen-precovered Ag(110) [26]. Furan reacted to produce CO_2 and H_2O as major products, as well as maleic anhydride, bifuran, and benzene.

In the present work, the reactivity of furfuryl alcohol and furan on oxygen-precovered Pt(111) was studied. Pt is of interest due to its use as a catalytic surface for aqueous phase oxidation due

to its corrosion-resistance in acidic conditions[27], relevance in organic electro-oxidation applications such as direct alcohol fuel cells[28,29], and reactivity of furanic compounds in thermochemical conditions [30,31]. While these systems are complex, it would be useful to understand the elementary steps involved in oxidation of furanic compounds to value-added products. The present study utilized TPD, HREELS, and density functional theory (DFT) to determine reaction paths of furanic species with surface oxygen. Moreover, the surface science results for furanic oxidation on Pd(111) [9] and Pt(111) were used to explain observed selectivity trends in furfural electrocatalytic oxidation on Pd and Pt catalysts.

Methods

Surface Science Experiments. Both TPD and HREELS experiments were conducted in ultrahigh vacuum (UHV) systems described in detail in previous publications [32,33]. Briefly, TPD experiments were performed in a chamber equipped with a Smart-IQ+ quadrupole mass spectrometer (VG Scienta). Fragmentation patterns for all relevant species were obtained either by recording a mass spectrum during exposure or from the multilayer desorption spectrum. The Pt(111) sample (Princeton Scientific) was mounted on tantalum foil which was spot-welded to two tantalum filaments. The temperature was monitored by a spot-welded thermocouple placed between the sample and the tantalum foil backing.

In this chamber, the sample was cooled through thermal contact with a liquid nitrogen reservoir. Furfuryl alcohol was dosed onto the surface using a direct dosing line pointed at the sample surface and exposure-dependent measurements were conducted by varying the pressure in the dosing line and tracking the change in the chamber pressure after dosing.

HREELS experiments were performed in a chamber equipped with an LK model ELS3000 high-resolution electron energy spectrometer (LK Technologies) and a model 981-2046 sputter gun

(Varian) for cleaning. The Pt(111) sample was mounted on a 1.5 mm tantalum disk and held onto a copper stage using two metal clips. The temperature was measured using a thermocouple which was welded onto the stage directly adjacent to the tantalum disk. HREELS experiments were conducted at a specular angle of 60° with respect to the surface normal. To study the thermal chemistry, the crystal was annealed at various temperatures for a few seconds and then cooled before collecting spectra. Cooling below room temperature was accomplished through a liquid nitrogen-cooled air line located in thermal contact with the sample backing.

The HREELS and TPD chambers utilized different sample holders. Whereas the HREELS system employed a mount with a more remote thermocouple for ease of sample transfer, the TPD system was designed for better temperature control via direct contact of the thermocouple with the Pt surface. The more remote thermocouple location on the HREELS system resulted in lower temperature readings compared to the TPD system, as determined by the desorption temperature of CO, which was lower by approximately 50 - 80 K.

Both chambers operated at a base pressure of approximately 10^{-10} Torr. The Pt(111) crystals were cleaned primarily through cycles of cooling and heating in 1×10^{-7} Torr O_2 between 373 and 900 K. When this cleaning method was insufficient, mild sputtering with Ar^+ ions (1 - 3 keV) and annealing at 900 K was used.

Furfuryl alcohol and furan were obtained from Sigma-Aldrich at 98% and 99% purity, respectively, and were further purified using repeated freeze-pump-thaw cycles. Ultrahigh-purity O_2, CO, and Ar^+ were obtained from Matheson Trigas.

Computational Methods. DFT calculations were used to predict vibrational frequencies of possible adsorbed intermediates and for investigating the energetics of oxidation steps to help clarify plausible furanic conversion paths. DFT calculations were performed within the Vienna

Ab initio simulation package (VASP, version 5.4.4), using the periodic supercell approach [34]. The projector augmented wave (PAW) method was used for electron-ion interactions [35]. The Perdew-Burke-Ernzerhof functional described the electron-electron exchange and correlation energies [36]. A plane wave basis set was used with an energy cutoff of 450 eV. For geometry optimization, the convergence criteria of the forces acting on atoms was 0.05 eV $Å^{-1}$, while the energy threshold-defining self-consistency of the electron density was 10^{-5} eV. All calculations were performed on a 3 x 3 unit cell of Pt (111) with five atomic layer thickness and the bottom three layers frozen. For gas phase species (H_2O and CO_2), a cubic unit cell of 20 Å was used to calculate the energy of isolated molecule in vacuum. ZPVE corrections were added to both gas phase and surface adsorbates for calculating relative energetics of possible intermediates.

Density functional perturbation theory linear response calculations were performed to calculate the Born effective charge matrix (BEC), which is utilized to calculate the vibrational intensities of optimized intermediate structures based on the method developed by Gianozzi & Baroni[37]. Displacement modes associated with metal atoms were neglected in vibrational calculations. The resulting frequencies were then scaled by a factor of 0.97 to improve alignment with experimental data.

The relative energy of various feasible intermediates was compared based on a consistent reference of the gas phase initial reactant and the balance number of oxidizing moieties (O*) in separate unit cells. In addition, to observe the effect of co-adsorbed oxygen on the relative favorability, all furanic species were modeled with one oxygen atom co-adsorbed per unit cell. Multiple co-adsorption configurations were considered, with the goal of placing the furanic species in its preferred orientation and the O atom in a consistent minimum that did not involve metal atom sharing with the furanic species and was generally proximate to the functionalities being oxidized

in subsequent steps. The complex structure of the adsorbates and co-adsorption arrangement makes it difficult to assure all structures represent global minimum energy structures. We illustrate all reported adsorption configurations in the Supplementary Information(Fig S13).

The reaction energies for elementary dehydrogenation reactions were computed as converting the H atom and ½ of a surface adsorbed O* atom (in a separate unit cell) to produce ½ a water molecule, as reaction of surface adsorbed H* with adsorbed oxygen is expected to be fast under the relevant experimental conditions.

Relative energies with respect to gas phase furan or furfuryl alcohol as a reference state have been reported in Table S3 and S4. The variation of the binding strength due to co-adsorption of O* at1/9ML coverage has been reported in Table S5. Though we have considered O* and furanic species co-adsorption, the 3x3 unit cell and use of a separately adsorbed O* species as reactants suggest our energetics represent low coverage values. Thus, the reported energetics may not match the coverages present during the TPD and HREELS studies, and higher coverage of O* may reduce oxidation barriers and make oxidation reaction energies more favorable due to the repulsive interactions among O* species at high coverage.

Electrochemical Experiments. Electrochemical oxidation of 100 mM furfural (Sigma Aldrich, purified via vacuum distillation) in 0.25 M perchloric acid (Suprapure, Millipore Sigma) was carried out in a differential packed-bed electrochemical reactor. Complete details can be found in Ref 53. Briefly, an ink containing either 40% Pt/C (Premetek) or 40% Pd/C (Premetek) was deposited onto on porous carbon cloth and served as a flow-through working electrode. Electrochemically-active surface area was determined via underpotential-deposited hydrogen stripping. Steady state was established with a potentiostatic hold for 30 min, followed by sample collection for another 30 min. An RHE reference electrode and Pt counter electrode (both flame

polished) were located in bridge tubes that met the flow channel by tapped ports. Another port permitted gas phase analysis by membrane-inlet, online electrochemical mass spectrometry (OLEMS). The solution phase products observed at the outlet were characterized using LC/MS-APCI (Atmospheric Pressure Chemical Ionization) and NMR. UV-DAD (Diode Array Detector) measurements were used to quantify the identified products: furoic acid (251 nm), 5-hydroxy-2(5H)-furanone (200 nm), and maleic acid (215 nm). 5-Hydroxyfuroic acid was quantified via H-NMR using DSS as an internal standard. After confirming no other products except CO_2 could be detected by LCMS, OLEMS, or NMR, CO_2 was assigned to the remaining electron balance.

Results and Discussion

Surface Chemistry of Furan. The oxidation chemistry of furan was studied by first saturating the Pt(111) surface with O_2, yielding a surface covered with ¼ monolayers of O atoms, hereafter referred to as O/Pt(111)[8,38,39]. Figure 1 shows the TPD spectrum of a saturating dose of furan on ^{18}O/Pt(111). Surface oxygen (which can be tracked based on the isotopic ^{18}O) was incorporated into H_2O, CO, and CO_2 products. Decomposition reactions to CO, CO_2, and H_2O were the dominant processes, while small amounts of benzene and H_2 were produced as well. Trace signals (such as $m/z = 29$) from other products in the temperature range around 400 – 450 K were detected, however, the intensities were too low to identify those products. This is discussed in detail below.

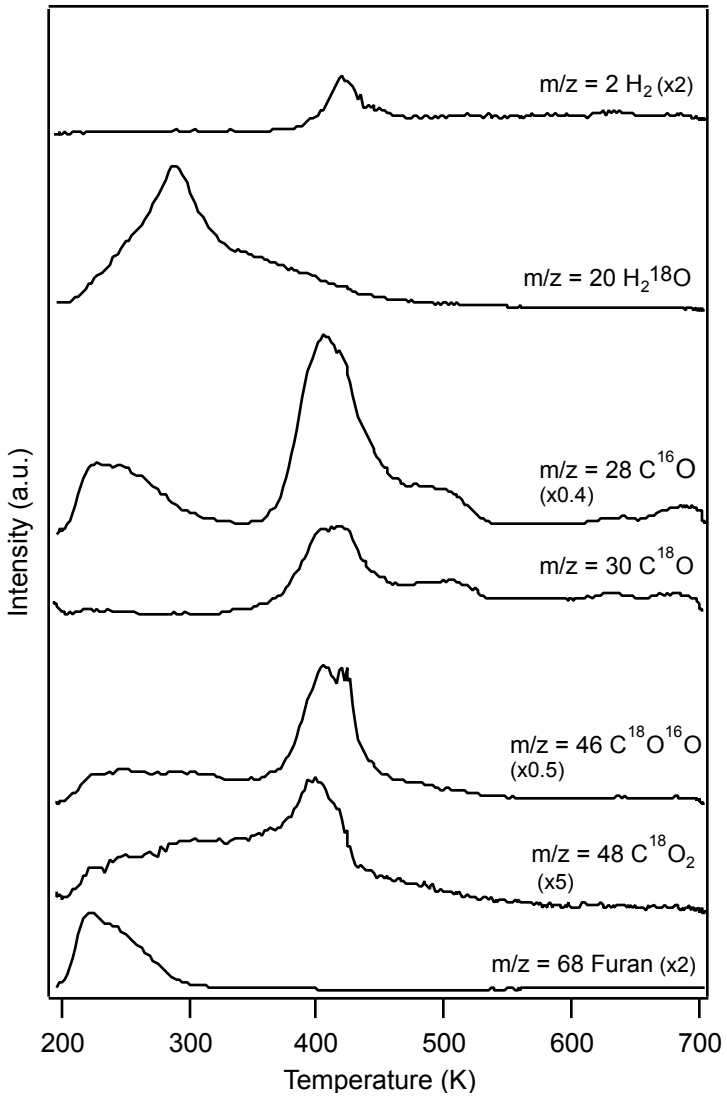

Figure 1. Thermal desorption spectra of furan on ^{18}O/Pt(111) dosed at 200 K.

Isotopic water, $H_2{}^{18}O$ (*m*/*z* = 20), hypothetically formed by the oxidation of surface H atoms generated during dehydrogenation reactions, desorbed in a peak around 290 K. The desorption peak was broad and largely occurred after furan molecular desorption, suggesting a variety of surface C—H scission processes that liberate H for the reaction. Desorption of $C^{18}O^{16}O$ occurred in two peaks at 407 K and 421 K. This is similar to CO oxidation on Pt(111), where CO_2 that was formed through interactions with atomic oxygen desorbed in three peaks[40]. $C^{18}O_2$ desorbed in a single peak at a lower temperature (398 K) than $C^{18}O^{16}O$, indicating that formation of CO_2 from

two surface oxygen addition steps may be associated with a kinetically distinct oxidation process. $C^{18}O$ desorption occurred at the same temperature as $C^{16}O$ desorption, indicating that both peaks originate from desorption-limited processes; however, desorption of labeled $C^{18}O$ indicates an earlier surface oxidation step that preceded desorption. Unlabeled products such as $H_2{}^{16}O$ and $C^{16}O_2$ (Supporting Information Figure S1) were attributed to desorption of water from the sample stage and contaminating unlabeled oxygen.

On clean Pt(111), we previously showed that furan did not undergo decomposition, but rather molecularly desorbed between 210 and 310 K, depending on the surface coverage[24]. Thus, the surface oxygen appeared to facilitate lower-barrier oxidation paths that were not available in the absence of oxygen. The decreased barriers for furan activation on the O-precovered surface were confirmed using HREEL spectroscopy in the present study. HREEL spectra collected after 6 L exposures of furan on Pt(111) and O/Pt(111) are shown in Figure 2 and corresponding vibrational assignments are in Table 1. For the clean Pt(111) surface, furan remained intact at low temperature, as indicated by intense C—H in-plane bending at 756 cm^{-1} and C—H wagging at 607 cm^{-1}. Upon heating to 218 K, these peaks decreased in intensity and no new peaks emerged, indicating the onset of molecular desorption. Further heating resulted in the disappearance of C—H and ring vibrations and indicated that furan did not react on clean Pt(111).

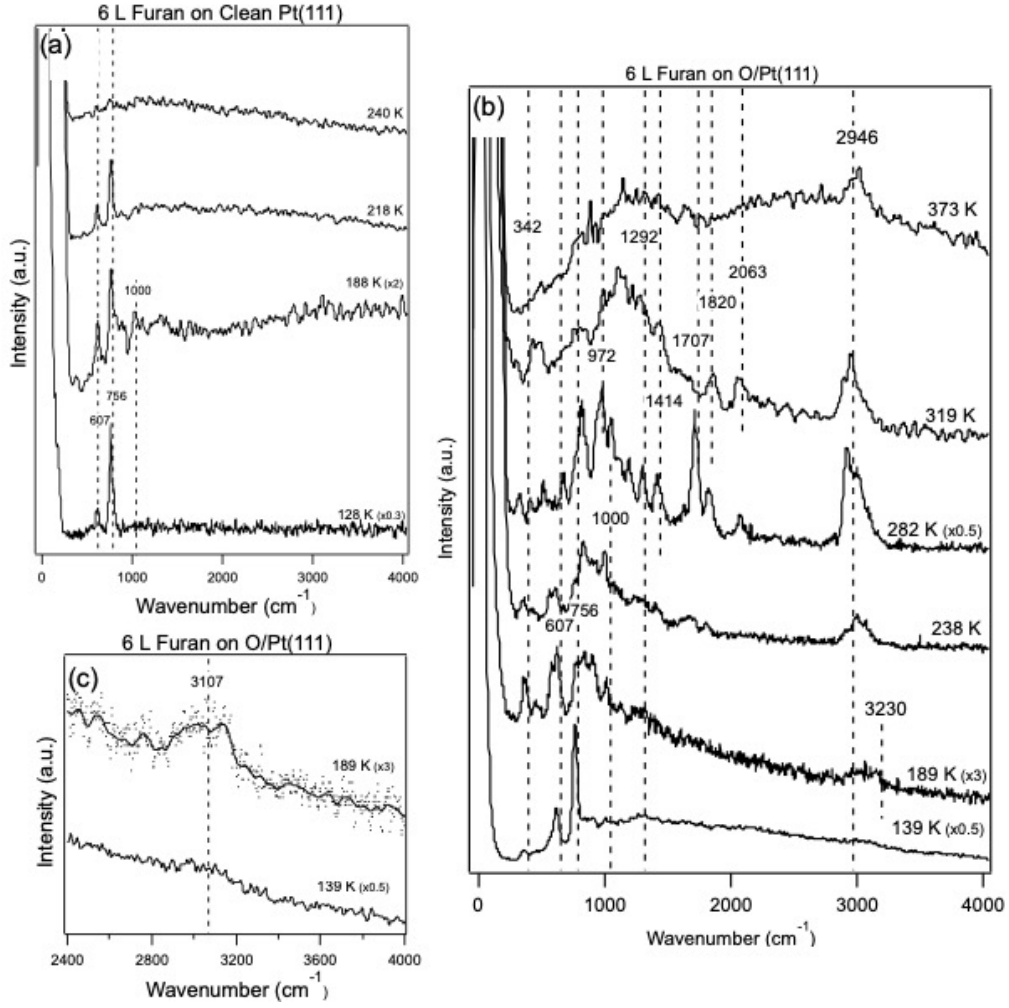

Figure 2. HREEL spectra of a high coverage 6 L furan exposure on (a) clean Pt(111) dosed at 128 K, (b) O/Pt(111) dosed at 139 K, and (c) a magnified portion of the 139 K and 189 K scans from panel (b). Each system was annealed briefly to the temperatures as noted. Spectra have been normalized to the elastic peak height.

Table 1. Vibrational Mode Assignments (cm^{-1}) of Furan Adsorbed on O/Pt(111) Compared to Clean Pt(111), O/Pd(111), Clean Pd(111), and in the Vapor Phase

Mode	Furan O/Pt(111)	Furan clean Pt(111)	Furan O/Pd(111) [9]	Furan clean Pd(111) [20]	Furan IR vapor [41]
Ring ν(CH)	3000-3160	n.r.	3050-3100	3085	3140, 3167

Ring ν(C—O)	n.r.	n.r.	1700	1750	n.r.
Ring ν(C—C)	n.r.	n.r.	1400	1445	n.r.
ν(ring)	1292	n.r.	n.r.	1005	1384, 1491
δ(CH)	1000	n.r.	n.r.	1005	995, 1066
δ(ring)	850	n.r.	n.r.	n.r.	871
γ(CH)	756	756	750	750	n.r.
γ(ring)	607	607	505	540	n.r.

In contrast, furan reacted to form a variety of surface-bound intermediates on O/Pt(111), as shown by the HREEL spectra in Figure 2b. At low temperature, furan molecularly adsorbed and two distinct peaks for ring out-of-plane bending, 607 cm^{-1}, and C—H wagging, 756 cm^{-1}, emerged, as well as a broad but small feature around 2900-3230 cm^{-1}, indicative of ring C—H stretching. After heating to 189 K, new losses appeared; these were assigned to ring wagging at 342 cm^{-1}, ring in-plane deformations in a broad peak centered at 850 cm^{-1}, ring C—O stretching at 1000 cm^{-1}, ring stretches at 1292 cm^{-1}, and ring C—H stretches within a broad peak around 2900-3230 cm^{-1}. The presence of these modes indicated that the C—H bonds were stretching out-of-plane with the ring, however the molecule remained flat-lying on the Pt surface (Figure S13). The peaks at lower wavenumbers indicated an intact ring at this temperature, but the difference between the low-temperature scan and that at 189 K suggested the possible onset of reaction.

To help identify surface bound reaction intermediates, we carried out DFT vibrational frequency and intensity calculations for optimized furan-derived species on Pt(111). The DFT-derived IR spectra showed good alignment between an oxidized furan species and the HREEL spectra at 189 K. Furyl intermediates were also found to be plausible based on DFT-IR calculations (Table S1), but were considered less likely based on TPD measurements and reaction path calculations. The

TPD results (Figure 1) indicated that surface-produced water, $H_2{}^{18}O$, did not desorb until about 280 – 300 K, which was significantly higher than the temperature at which surface reactions began in HREELS (Figure 2b). If the furan ring was initially activated through oxygen-assisted dehydrogenation to furyl intermediates, one would expect water formation and desorption at low temperatures based on prior observations on Pt(111) surfaces[42]. The DFT-calculated activation barrier for direct oxygen addition to the furan ring is also 0.20 eV lower than surface oxygen assisted C-H dissociation (Supporting Information Figure S9). We therefore conclude that direct oxygen addition is the likely first reaction step; this point is addressed in further detail below.

Upon heating to 238 K, the HREEL spectrum (Figure 2b) showed the appearance of a new, more intense C—H stretching peak at 2946 cm^{-1}, signaling that further reaction had taken place. An emerging peak at 1668 cm^{-1} was consistent with a C=O function formed from the addition of an O at the alpha carbon. Changes in the lower-frequency structure of the spectrum also suggested formation of a new reaction intermediate(s).

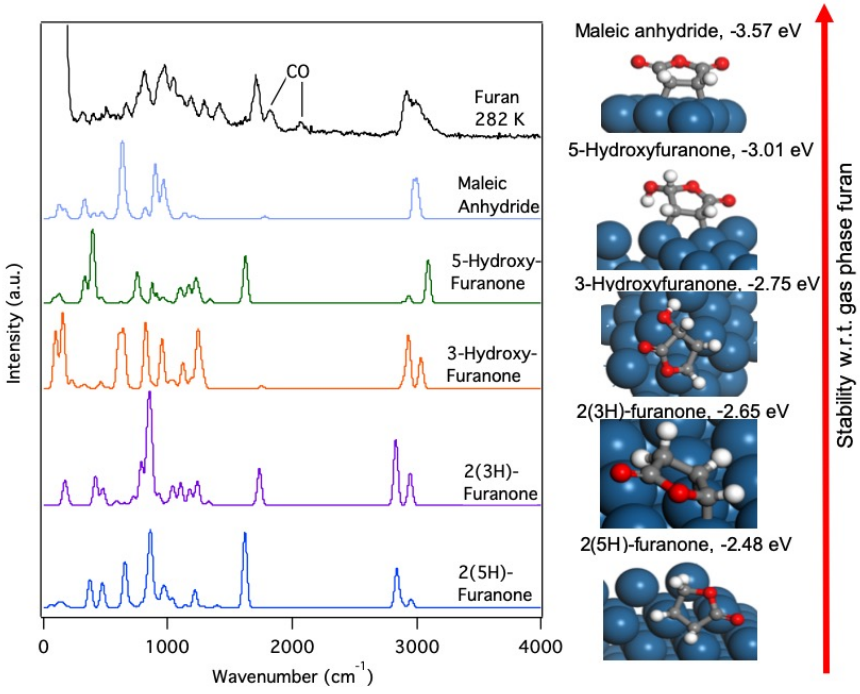

Figure 3. HREEL spectra of furan on O/Pt(111) (black) annealed at (a) 282 K compared to calculated reaction intermediate vibrations for the 2(3H)-furanone (purple), 2(5H)-furanone (blue), 3-hydroxyfuranone (orange), 5-hydroxyfuranone (green), and maleic anhydride (violet) on Pt(111). (b) DFT calculated structures for the most stable adsorbed oxidized intermediates and their relative energies with respect to gas-phase furan.

Increasing the surface temperature further to 282 K resulted in spectral features strongly indicative of C=O formation and the onset of decarbonylation. In particular, a strong loss at 1707 cm^{-1} emerged, which is assigned to a C=O stretch within an oxidized furanic intermediate. Smaller peaks at 1820 cm^{-1} and 2063 cm^{-1} were assigned to surface CO and implied the onset of decarbonylation. The spectrum at 282 K aligned relatively well with DFT calculated spectra for a variety of oxidized species such as adsorbed 5-hydroxyfuranone (5OHF), 3-hydroxyfuranone (3OHF), 2(3H)-furanone (23HF), 25HF, and maleic anhydride (MA) (Figure 3, Table S2). The more oxygenated intermediates, such as 3OHF and MA, were less likely to be present due to the lack of a C=O mode around 1707 cm^{-1} in their DFT-IR spectra that is apparent in the experiment. However, 5OHF was found to have a strong loss at 1700 due bending of the C=O bond towards the surface. Previous studies of 25HF suggested that it should not be stable at this temperature on Pt(111), and the overall structure of the C—H stretching region (around 2950 cm^{-1}) and location of the C=O mode, indicates that 23HF is in the best agreement with the experimental spectrum (Figure 3)[43]. We note that 23HF was also observed as a product in electrochemical oxidation of furfural on Pt catalysts at potential of 1.0V and higher.[53] As discussed below, surface 23HF was also found to be a reasonable intermediate based on its formation energy. However, the formation of other furanone-type species cannot be ruled out.

At 320 K, the HREEL spectrum in Figure 2b showed the disappearance of the carbonyl peak at 1707 cm^{-1}, indicating the conversion of furanone intermediates. Moreover, the spectrum lacked clear ring features below 1000 cm^{-1}; we therefore conclude that ring-opening of furan had occurred by this temperature, though the breadth of the observed peaks suggested that a complex mixture of intermediates may have been formed. Peaks at 972, 1096, 1218, 1292, and 1420 cm^{-1}, were consistent with various C—C and CH_X vibrations[44]. By 373 K, the removal of CO was observed, as indicated by the lack of vibrations at 1820 and 2063 cm^{-1}, though a variety of poorly-resolved carbonaceous fragments appeared to persist on the surface.

Surface Chemistry of Furfuryl Alcohol. To understand how substitution of the furan ring influenced oxidation, we also studied the reaction of furfuryl alcohol on O/Pt(111). As shown in Figure 4, the dominant products observed by TPD were CO, CO_2, and H_2O, consistent with extensive oxidation. Previous studies on clean Pt(111) revealed that furfuryl alcohol largely underwent decarbonylation and decomposition to produce furan, propylene, CO, and benzene, where furfural acts as an intermediate for furan production [23,24,45]. In addition, furfuryl alcohol underwent deoxygenation at high reactant coverages[13,46]. We observed smaller quantities of the same products on O/Pt(111) (Supporting Information Figure S4), with the addition of small peaks in m/z = 54 and m/z = 55 attributed to trace quantities of MA and furanone compounds, respectively (Figure S4). The low peak intensities suggested that formation of these products might be attributed to surface defects. (Note that the intensities for other C_{4+} products, particularly methyl furan and furan, were also low.). The low yield of C_{4+} products in comparison with FA chemistry on clean Pt(111) suggested that reactions with surface O ultimately led to substantial ring decomposition.

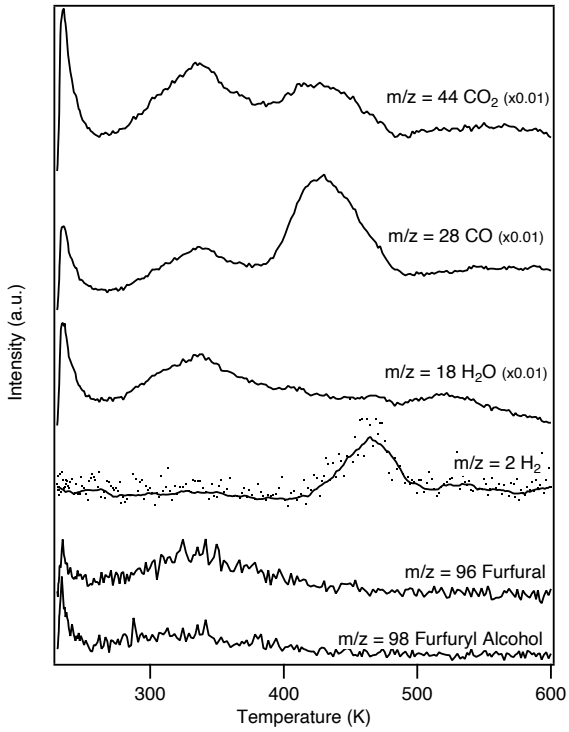

Figure 4. Thermal desorption spectra of furfuryl alcohol on ^{16}O/Pt(111) dosed at 230 K. Moving averages were calculated for H_2 due to noise involved in the spectra (the raw data are shown as points) and trace products are reported in Supporting Information Figure S4.

HREELS was also used to study the surface reaction pathways for furfuryl alcohol on O/Pt(111). Figure 5 shows the HREEL spectra collected after a 2.5 Langmuir exposure of furfuryl alcohol on both clean Pt(111) and O/Pt(111) at low temperatures and corresponding peak assignments are in Table 2. Complete peak assignments and analysis of the clean surface were reported previously [24] and are briefly summarized here. On clean Pt(111), heating from 133 K to 203 K resulted in the disappearance of the O—H stretch at 3500 cm^{-1}, which indicated that furfuryl alcohol underwent dehydrogenation to produce a surface alkoxide by 203 K. Increasing the surface temperature resulted in the evolution of a surface aldehyde C=O stretch at 1690 cm^{-1}, which suggested further dehydrogenation of the alkoxide to create a surface aldehyde between 220 and 251 K. The presence of surface CO losses at 1831 and 2968 cm^{-1} indicated that the aldehyde began undergoing

decarbonylation by 251 K to create a furyl intermediate (C_4H_3O). Prior TPD studies proposed that the furyl intermediate underwent decarbonylation to create a C_3H_x intermediate[24].The spectra at 273 K also indicated the onset of decomposition which was indicated by the lack of resolved intact furyl ring features at 925, 1232, 1314, and 3145 cm^{-1}. Further heating to 340 K allowed for the evolution of peaks at 814, 1120, 1425, and 3005 cm^{-1} which correspond to benzene-like C—C and C—H modes on Pt(111) [47]. This indicated that at 340 K, C_3H_x intermediates underwent a coupling reaction which created benzyl-like intermediates.

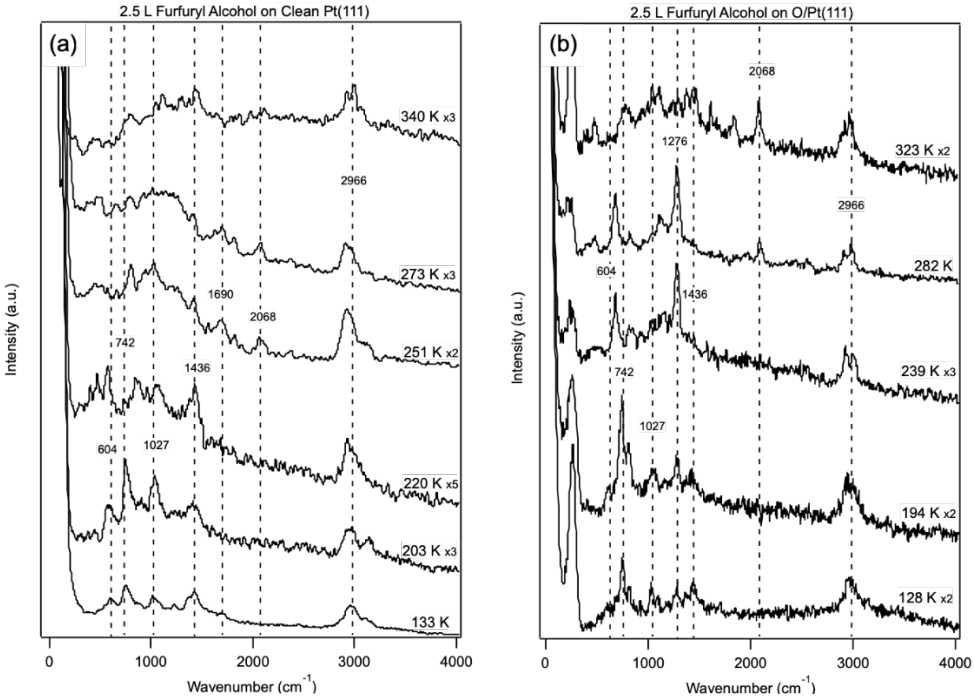

Figure 5. HREEL spectra of a high coverage 2.5 L furfuryl alcohol exposure on (a) clean Pt(111) at dosed at 133 K and is reported in Mark, et. al. [24], and (b) O/Pt(111) dosed at 128 K. Each system was annealed briefly to the temperatures as noted. Spectra have been normalized to the elastic peak height.

Table 2. Vibrational Mode Assignments (cm^{-1}) of Furfuryl Alcohol Adsorbed on O/Pt(111) Compared to Clean Pt(111), Clean Pd(111), Liquid Phase, and in the Vapor Phase

Mode	Furfuryl alcohol O/Pt(111)	Furfuryl alcohol clean Pt(111) [24]	Furfuryl alcohol Pd(111) [9]	Furfuryl alcohol liquid IR [48]	Furfuryl alcohol IR vapor [48]
δ(CCO)	n.r.	414	450	420	421
Ring γ(CH) or τ(C=C)	604	604	n.r.	740, 814, 885, or 597	732, 743, 810, 889, or 599
$\varrho_r(CH_2)$	742	760	780	740	732
ν(C-C) or δ(CH)	n.r.	925	900-925	956, 1010	955, 1019, 1024
$\tau(CH_2)$	1027	1019	n.r.	1077	n.r.
ν(C=O) side group	n.r.	n.r.	n.r.	1055	n.r.
ν(C-C), ν(ring)		n.r.	1150	1148	1155
$\varrho_{as}(CH)$, $\chi_{as}(CH)$	1276	1232	n.r.	n.r.	n.r.
ν(ring)		1314	1395	1361, 1379	1381
CH_2 deformations/$\chi(CH_2)$	1436	1425	n.r.	1450	1462
ν(C=C)	n.r.	n.r.	n.r.	1503, 1599	1508, 1600
$\nu_S(CH_2)$	n.r.	n.r.	2875	2870	2880
$\nu_a(CH_2)$	2966	2960	n.r.	2928	2938
Ring ν(CH)	n.r.	3140	3075	3123, 3150	3121, 3159
ν(OH)	3000-3160	3510	3250	n.r.	3652, 3660

For O-precovered Pt(111), furfuryl alcohol adsorbed intact and in a multilayer state at 128 K, with methylene modes at 742 cm^{-1} and 2966 cm^{-1}, as well as a broad O—H stretch near 3500 cm^{-1} (for DFT-IR comparison, see Supporting Information Figure S5). Further, ring wagging and twisting at 604 cm^{-1} and furan ring stretching, apparent in a shoulder at 1361 cm^{-1}, indicate an intact molecule.

Heating to 194 K brought about minor changes to the spectra. An increase in intensity at 742 cm^{-1} indicated relatively more intense methylene rocking, perhaps signaling the desorption of multilayer furfuryl alcohol. The O—H stretch near 3500 cm^{-1} disappeared by this temperature, consistent with initial dehydrogenation of the adsorbed alcohol to produce a surface alkoxide intermediate, similar to what was seen on the clean Pt(111)[49]. Further, at 194 K, methylene CH_2 stretching (742 and 2966 cm^{-1}) remained intense, further indicating the formation of an alkoxide rather than hydroxyfuryl intermediate in the first mechanistic step. DFT-calculated spectra for thermodynamically stable flat-lying alkoxide and a less stable vertically adsorbed alkoxide align well with the spectrum at 194 K (Supporting Information Figure S6).

On the clean surface, further heating to about 250 K resulted in decarbonylation of the surface species. Heating the FA-dosed O/Pt(111) surface to 239 K and 282 K yielded spectra distinct from those obtained on the clean surface. Minor losses between 700 and 1100 cm^{-1} indicated an intact furyl ring, while a sharp peak emerged at 676 cm^{-1} from an existing shoulder in the lower temperature spectra and was indicative of ring stretching. The intense methylene rocking loss at 742 cm^{-1} disappeared at this temperature and the peak at 2966 cm^{-1}, which was indicative of methylene stretching, was replaced by two weaker losses, indicative of ring C—H stretching at various C atoms at 2933 and 3024 cm^{-1}. The reduction in methylene stretching intensity at this temperature indicated likely dehydrogenation. However, at this temperature there was no surface C=O stretch, as indicated by the absence of a loss around 1700 cm^{-1}. This suggested that the intermediate produced from the dehydrogenation at the methylene was not a surface aldehyde. Further, a peak at 1276 cm^{-1}, which existed in the lower temperature spectra as a weak loss, gained intensity at 239 K and 282 K. A loss at a similar frequency in the low-temperature spectrum was assigned to asymmetrical ring C—H vibrations; however, previous studies have shown the

disappearance of this mode at this temperature due to ring dehydrogenation[24,45]. Further, the presence of oxygen suggested that the loss was likely indicative of the O—C—O vibration of a strongly bound carboxylate, which suggested the onset of oxidation of the surface intermediates. This frequency is somewhat lower than that typically assigned for carboxylate species, which are typically closer to 1350 cm^{-1} [48–50].

We investigated furoate adsorption on Pt(111) using DFT calculations. DFT calculations predicted that the OCO stretching frequencies depended on orientation. For the thermodynamically most stable flat-lying orientation (Figure 6), a relatively intense stretch of the C—O bond in the OCO functional group was found at 1186 cm^{-1}, while the less stable bent furoic acid intermediate had a C—O stretch on the carboxylate group at 1225 cm^{-1}. For the least stable vertical intermediate, intense OCO stretching modes were at 1430 cm^{-1}, closer to that traditionally expected for carboxylate species. Overall, the DFT calculations indicate that the pendant furyl ring can profoundly influence carboxylate adsorption structure, thus red-shifting OCO peaks (Supporting Information Figure S7).

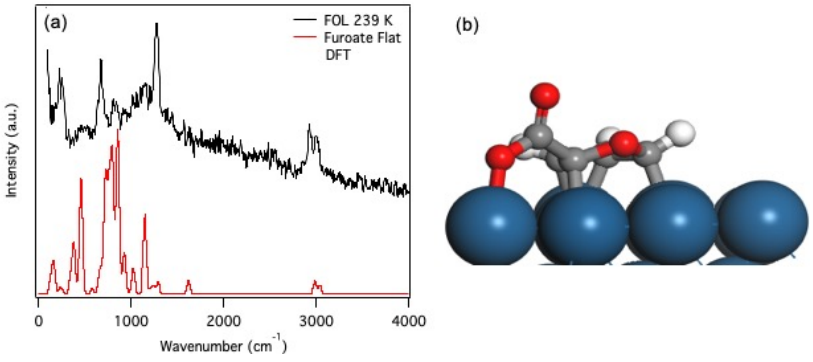

Figure 6. HREEL spectra for furfuryl alcohol on O/Pt(111) annealed at 239 K (black) compared to calculated vibrations and intensities for furoate on Pt(111) in a (a) flat-lying orientation and (b) the DFT optimized structure for furoate in a flat orientation.

Decarboxylation of the proposed furoate intermediate occurred by 323 K and produced CO_2, as seen in the TPD results in Figure 4. Decarbonylation intermediates likely decomposed around this temperature as well, as indicated by the strong surface CO losses at 1850 cm^{-1} and 2068 cm^{-1} (Figure 5). The broadness of the spectra indicated a variety of surface species. Notably, while furoate decarboxylation was expected to produce adsorbed furyl and derivative products equivalent to those seen in furan TPD, the high-temperature HREEL spectrum at 323 K was notably different than the furan spectra at all temperatures. The 323 K spectrum for furfuryl alcohol, unlike higher-temperature scans, was not broad. This suggested a large concentration of the furyl intermediate on the surface. The difference between the 323 K furfuryl alcohol spectra and the furan spectra at a variety of temperatures indicated that furan reactions on oxygen-precovered Pt(111) likely did not proceed through an adsorbed furyl, as proposed above.

Reaction Path Analysis Based on UHV Studies and DFT Calculations. The thermodynamic stabilities of key oxidation intermediates of furan and furfuryl alcohol on oxygen-covered Pt (111) were computed using DFT methods. The relative energies of surface-bound species were determined with respect to gas phase furan or furfuryl alcohol, as described in detail in the Supporting Information (Table S3 and S4). Reaction energy diagrams are shown in Figs. 7 and 8 to show the thermodynamically favored oxidation path for comparison to experimentally observed oxidation surface intermediates. In these diagrams, reaction energies are shown with few activation barriers; thus, differences in barriers for parallel steps could lead to a less stable intermediate being preferred under the experimental conditions.

The reaction energetics for oxidation of furan on O-covered Pt (111) are shown in Figure 7. As discussed above, the TPD and HREEL data, together with initial step DFT barriers and frequency results (Supporting Information Figure S2) are most consistent with the initial step being addition

of surface O to the ring. This oxidized intermediate was found to be thermodynamically feasible, with an exothermic reaction energy of -0.19 eV from adsorbed furan (Figure 7). Further, this intermediate has a smaller activation barrier (by 0.2 eV) for formation than oxygen assisted C—H bond scission (Figure 7). This activation barrier was also smaller than the C—H dissociation barrier in the absence of oxygen (Supporting Information Figure S9). HREEL spectra indicated that this oxygenated furan reacted by 282 K to produce a furanone intermediate, as evidenced by the appearance of a sharp peak near 1700 cm^{-1} (Figure 2(b)). The most straightforward way to produce furanone is via H migration between the C^2 and C^3 position of the furan ring. Although this step is computed to be thermodynamically downhill, we were unsuccessful in identifying a reaction path with a barrier less than 1.4 eV at low coverage. However, we note that there is precedent for such hydride shifts at similar temperature, for example in formation of acetaldehyde from oxametallacycles derived from ethylene oxide on Ag(111)[51].

As shown in Figure 7, a variety of furanone-type species are energetically accessible, but the simplest interpretation of the results is that the dominant species at these temperatures are $C_4H_XO_2$ intermediates (such as 23HF) produced by a single O addition and hydride transfer step. Note that at temperatures of 325 K and above, experiments indicated that ring-opening and substantial decarbonylation of the furanic species had occurred; these reactions were not probed with DFT calculations, with many paths being available (some of which were considered in our previous publication)[52]. The onset of this decomposition occurred at lower temperatures, as evidenced by the appearance of CO stretching modes in the 282 K spectrum. This is consistent with a portion of the surface intermediates undergoing more substantial decomposition than the species shown in Figure 7; formation of these intermediates may involve C—H activation steps that could provide surface H for the reactions indicated in Figure 7.

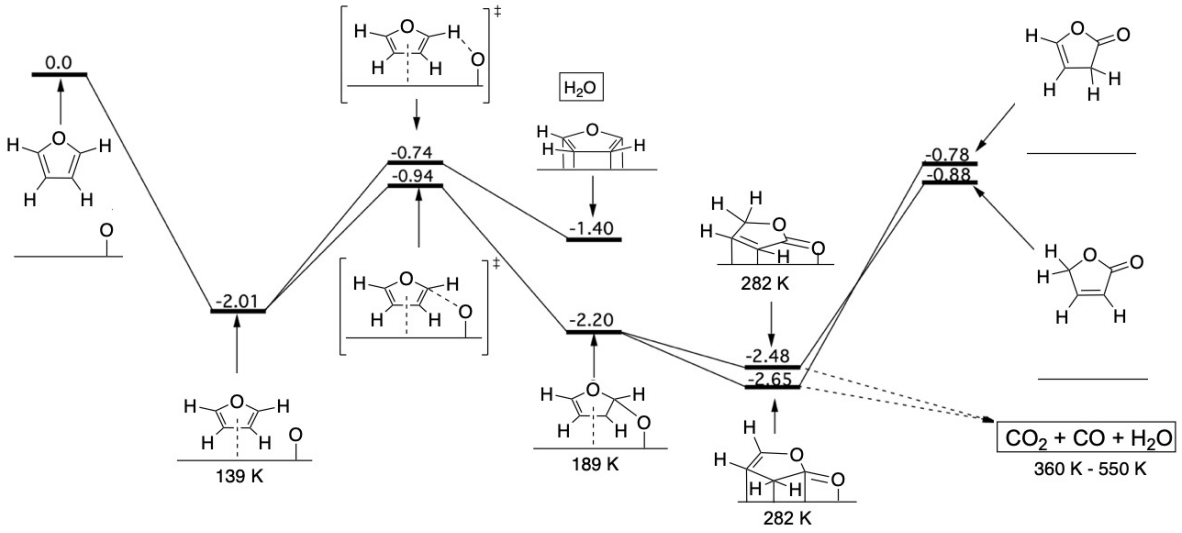

Figure 7. Potential energy diagram for furan oxidation to partially oxidized products 2(3H)-furanone and 2(5H)-furanone on Pt(111). Transition state energies for the initial step in the reaction are highlighted in red. Relative energies (in eV) are given to gas-phase furan and adsorbed O*, assuming that any water formed by an oxidation reaction desorbed from the surface. Oxidizing moieties are present in a separate unit cell. Temperatures for which isolation of intermediates or products were observed in experimental HREELS or TPD studies are shown below those species.

Figure 8 shows the reaction energetics for oxidation of furfuryl alcohol on oxygen-covered Pt (111). DFT calculations indicate that the initial O—H bond scission to produce an alkoxide intermediate is slightly uphill in energy when water is assumed to be the gas-phase product; if water is adsorbed, the reaction energy decreases by 0.15 eV. DFT-IR calculations indicated that both flat and vertically adsorbed alkoxide intermediates could have been present on the surface due to the similarity in the spectra (Supporting Information Figure S6), however the flat orientation was energetically more favorable at the low coverages considered in the DFT calculations.

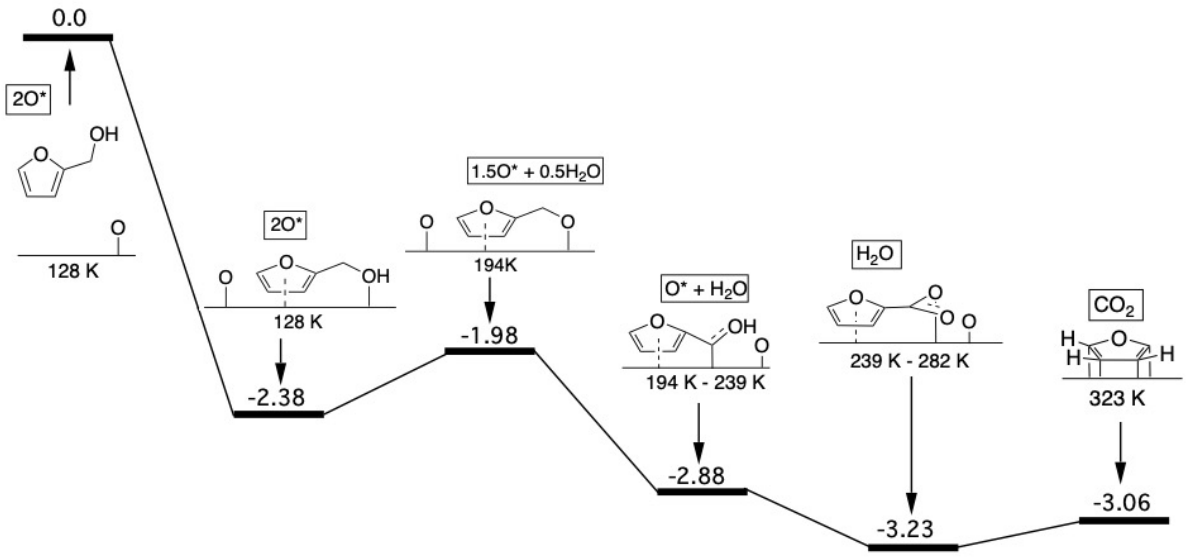

Figure 8. Potential energy diagram for furfuryl alcohol oxidation to furyl, which can then yield 2(5H)-furanone and 2(3H)-furanone, 5-hydroxyfuranone, 3-hydroxyfuranone, and maleic anhydride on oxygen-precovered Pt(111). Energies in eV are relative to gas-phase furfuryl alcohol and adsorbed atomic oxygen, with possible oxidizing moieties present in a separate unit cell.

The calculations revealed a strong enthalpic driving force for further dehydrogenation to a surface acyl, with an additional energy change of -0.90 eV; acyl oxidation to furoate was also downhill in energy, consistent with the above identification of furoate as a likely intermediate based on the 239-282 K HREEL spectra (Figure 5b). The fate of the furoate was difficult to determine based on the HREEL spectra due to the broadness of the spectra at high temperatures, which indicated a large variety of surface species. The DFT calculations suggested that furoate decarboxylation to produce a furyl intermediate, while releasing an equivalent of CO_2, was energetically feasible, consistent with production of CO_2 in the TPD experiments (Figure 4). This intermediate could undergo oxidation to produce furanone species similar to the routes described in Figure 7 (Supporting Information Figure S10). Energetics indicated that furyl oxidation to a

furanone species was downhill and further hydrogenation was moderately uphill in energy. The furyl intermediate can also oxidize to maleic anhydride and hydroxyfuranones (23OHF and 25OHF) (Supporting Information Figure S10). Out of the variety of partially oxidized species that could be formed from furyl, maleic anhydride was calculated to be the most energetically favored product and was also detected in trace amounts during TPD analysis (Supporting Information Figure S4) of furfuryl alcohol oxidation. Due to the low volatility of these oxidized surface species, a majority of these intermediates further convert to CO, CO_2, and H_2O prior to desorption. However, under steady state catalytic oxidation conditions carried out in aqueous solution, with potentially higher coverages of intermediates and surface adsorbed oxygen, we speculate that significant yields of such product could be observed. If oxidation is performed in a liquid phase, solvation could further motivate desorption of partially oxidized products.

DFT calculations reported here utilized co-adsorbed O in the unit cell to simulate an oxidizing environment for the furanic molecules. The presence of co-adsorbed O reduces the adsorption energy of most intermediates considered for this work (Supporting Information Table S5), however, the adsorption energy trends were not altered.

Implications for Catalytic Oxidation of Furanic Compounds. These findings have important implications for catalytic and electrocatalytic oxidation reactions involving furanic molecules. In particular, we propose here that furanone-type products are produced through direct oxygen insertion into a Pt-C bond in furan. Other studies have considered the oxidation pathways of furanic molecules on metal surfaces, such as Ag(110)[26] and Pd(111)[9]. Oxygen addition to furan or a furyl species occurred on Ag(110), where O attacks a furyl species at the C^2 carbon and decomposes to CO_2 and a surface C_3-species. On Pd(111), Williams, et al.[9] proposed that oxygen addition followed furyl ring-opening and the partially oxidized species were produced through ring closure.

In contrast, the electro-oxidation of furfural to furoic acid, 5-hydroxy-2(5H)-furanone, 5-hydroxyfuroic acid, and maleic acid, has been observed on Pt anodes, and oxygen-addition reactions have been proposed that are similar to those shown here[52,53]. The production of furanone-type molecules requires fewer steps on Pt(111) due to the lack of ring-opening required for oxidation to occur, suggesting that Pt is promising as an efficient catalyst for furanone and MA production.

To probe how differences in mechanisms translate to electrocatalytic oxidation behavior, we measured selectivity during the oxidation of furfural on Pd/C to complement the earlier, similar work on Pt/C catalysts[53]. A comparison of selectivities and faradaic efficiencies on the two catalysts is shown as Figure 9. The Pd catalyst was found to be more active toward furfural oxidation, with significant product yields detected at 0.8 V_{RHE}. Over Pt, significant currents were not observed until 0.9 V_{RHE}, and Figure 9 shows the comparison of selectivity at the onset of oxidation for the two materials. (For a comparison at the same potential, see Figure S12.) Both Pd and Pt produced furoic acid as the major product at mildly oxidizing potentials, as expected based on the surface science studies on Pd(111)[9] and Pt(111), which both showed oxidation to surface furoate via a low-barrier process. The Pd catalyst was not only more active at low potential, but also more selective to 5-hydroxy-furan-2(5H)-one, which was hypothetically formed via a pathway that requires initial C-C activation. This higher selectivity toward elimination of the pendant group appears to be consistent with the earlier appearance of surface-bound CO during temperature programmed reactions of furfural on O-covered Pd(111), which was detected at temperatures as low as 230 K.

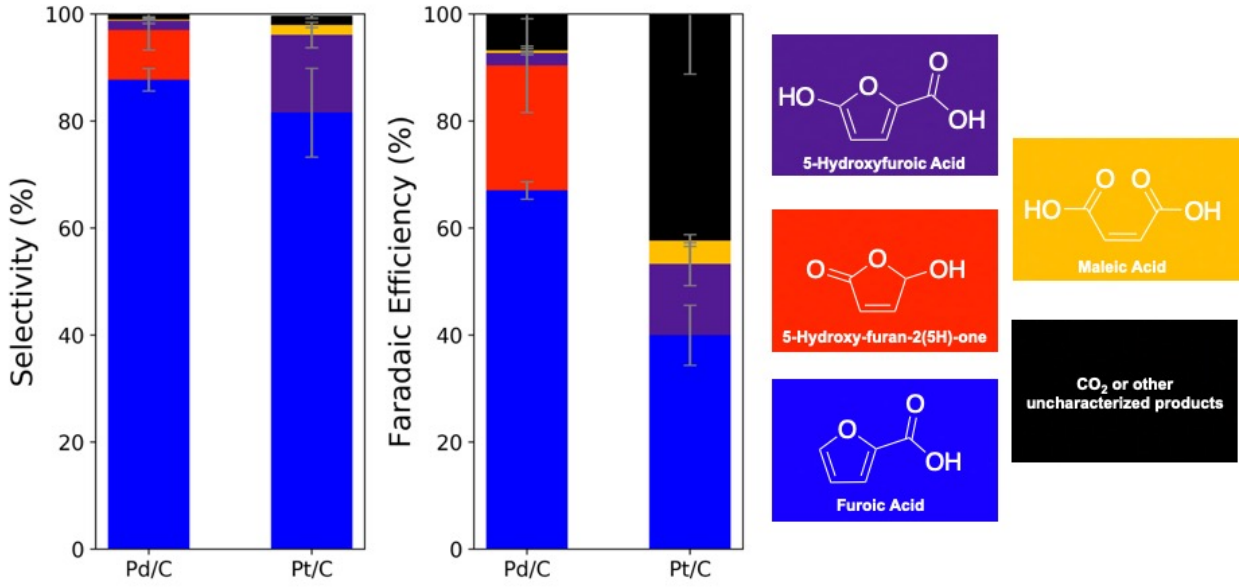

Figure 9. Product selectivity (left) and faradaic efficiency (right) to major products during furfural electro-oxidation at the onset potentials for oxidation of 0.8 V_{RHE} (Pd/C) and 0.9 V_{RHE} (Pt/C) in 0.25M $HClO_4$.

More interestingly, Pt was found to exhibit a much higher selectivity toward the product 5-hydroxyfuroic acid, which would likely be formed via direct O(H) addition to the furan ring. Such a process appears similar to the direct addition reactions observed for furan in the present work and suggests that Pt may be more effective for such O(H) insertion reactions. Note that although prior studies of furfural oxidation on Pt showed that potentials above 0.9 V_{RHE} led to high selectivities to more oxidized products including maleic acid, such processes were not studied here due to stability issues of Pd in the low-pH solution.

It is worth noting that the structure of the furanic reactant (in particular the presence or absence of an alcohol pendant group) drastically affects the oxidation reaction pathway. The work here has indicated that the oxidation at the ring and at the pendant group are possible, however the presence of the functional group appears to favor oxidation of the pendant group prior to any oxygen

addition on the ring. This result also appears to be in line with the furfural oxidation product slate shown by Figure 9.

Conclusions

The surface chemistry of furan and furfuryl alcohol on O/Pt(111) has been explored using TPD, HREELS, and DFT. Furan was found to decompose into CO_2, CO, and H_2O, differing from a lack of furan reactivity on clean Pt(111). HREEL spectra in combination with DFT calculations determined that the presence of oxygen on the surface lowered the activation barrier for furan reactivity. Furan underwent direct oxygen addition to the ring, likely followed by a C2 to C3 hydride shift to form a 25HF intermediate that ultimately decomposed. Furfuryl alcohol largely decomposed into CO_2, CO, and H_2O. Trace amounts of decarbonylation and deoxygenation products were detected, as well as partially oxidized products of 25HF and MA. HREELS and DFT results indicated that furfuryl alcohol was oxidized to a furoate intermediate in the presence of oxygen; this furoate reacted via decarboxylation to furyl intermediates. Overall, this work demonstrates that surface O addition to furanic compounds can occur directly on furan rings or on pendant oxygenated groups, with oxidation being steered toward the pendant group when it is present.

Supporting Information. Additional TPD and HREELS figures. Additional DFT calculated vibrational IR spectra and frequencies for furfuryl alcohol and furoate. Additional reaction energy diagrams for furan and furfuryl alcohol. Snapshots of the preferred adsorption geometries as determined by DFT for all molecules discussed in the text. This material is available free of charge on the ACS Publications website at DOI:

Corresponding Author
*Email: medlin@colorado.edu

Funding Sources
The authors would like to acknowledge the National Science Foundation (award number CHE-1665176) for funding.

Notes
The authors declare no competing financial interest.

Acknowledgments

L.O.M would like to thank the Graduate Assistance for Areas of National Need (GAANN) for financial support. This work used the Extreme Science and Engineering Discovery Environment (XSEDE), which is supported by National Science Foundation grant number ACI-1053575. NA acknowledges training provided by the Computational Materials Education and Training (CoMET) NSF Research Traineeship (grant number DGE-1449785).

References

(1) Huber, G. W.; Dumesic, J. A. An Overview of Aqueous-Phase Catalytic Processes for Production of Hydrogen and Alkanes in a Biorefinery. *Catal. Today* **2006**, *111*, 119–132.

(2) Corma Canos, A.; Iborra, S.; Velty, A. Chemical Routes for the Transformation of Biomass into Chemicals. *Chem. Rev.* **2007**, *107*, 2411–2502.

(3) Gallezot, P.; Richard, D. Selective Hydrogenation of a,B-Unsaturated Aldehydes. *Catal. Rev.* **2006**, *40*, 81–126.

(4) Gupta, K.; Rai, R. K.; Singh, S. K. Metal Catalysts for the Efficient Transformation of Biomass-Derived HMF and Furfural to Value Added Chemicals. *ChemCatChem* **2018**, *10*, 2326–2349.

(5) Eseyin, A. E.; Steele, P. H. An Overview of the Applications of Furfural and Its Derivatives.

Int. J. Adv. Chem. **2015**, *3*, 42–47.

(6) Li, X.; Jia, P.; Wang, T. Furfural : A Promising Platform Compound for Sustainable Production of C4 and C5 Chemicals. *ACS Catal.* **2016**, *6*, 7621–7640.

(7) Gallezot, P. Conversion of Biomass to Selected Chemical Products. *Chem. Soc. Rev.* **2012**, *41*, 1538–1558.

(8) Williams, R. M.; Medlin, J. W. The Influence of Oxygen on the Surface Chemistry of 1,2-Propanediol on Pd(111). *Surf. Sci.* **2014**, *619*, 30–38.

(9) Williams, R. M.; Pang, S. H.; Medlin, J. W. Ring-Opening and Oxidation Pathways of Furanic Oxygenates on Oxygen-Precovered Pd(111). *J. Phys. Chem. C* **2014**, *118*, 27933–27943.

(10) Williams, R. M.; Medlin, J. W. Benzyl Alcohol Oxidation on Pd(111): Aromatic Binding Effects on Alcohol Reactivity. *Langmuir* **2014**, *30*, 4642–4653.

(11) Kubota, S. R.; Choi, K.-S. Electrochemical Oxidation of 5-Hydroxymethylfurfural to 2 , 5-Furandicarboxylic Acid (FDCA) in Acidic Media Enabling Spontaneous FDCA Separation. *ChemSusChem* **2018**, *11*, 2138–2145.

(12) Cha, H. G.; Choi, K.-S. Combined Biomass Valorization and Hydrogen Production in a Photoelectrochemical Cell. *Nat. Chem.* **2015**, *7*, 328–333.

(13) Nam, D.; Taitt, B. J.; Choi, K. Copper-Based Catalytic Anodes To Produce 2,5-Furandicarboxylic Acid, a Biomass-Derived Alternative to Terephthalic Acid. *ACS Catal.* **2018**, *8*, 2–11.

(14) Lv, G.; Chen, S.; Zhu, H.; Li, M.; Yang, Y. Determination of the Crucial Functional Groups in Graphene Oxide for Vanadium Oxide Nanosheet Fabrication and Its Catalytic Application in 5-Hydroxymethylfurfural and Furfural Oxidation. *J. Clean. Prod.* **2018**, *196*, 32–41.

(15) Roylance, J. J.; Kim, T. W.; Choi, K.-S. Efficient and Selective Electrochemical and Photoelectrochemical Reduction of 5 -Hydroxymethylfurfural to 2 5-Bis (Hydroxymethyl)Furan Using Water as the Hydrogen Source. *ACS Catal.* **2016**, *6*, 1840–1847.

(16) You, B.; Liu, X.; Jiang, N.; Sun, Y. A General Strategy for Decoupled Hydrogen Production from Water Splitting by Integrating Oxidative Biomass Valorization. *J. Am. Chem. Soc.* **2016**, *138*, 13639–13646.

(17) Vuyyuru, K. R.; Strasser, P. Oxidation of Biomass Derived 5-Hydroxymethylfurfural Using Heterogeneous and Electrochemical Catalysis. *Catal. Today* **2012**, *195*, 144–154.

(18) Janik, M. J.; Taylor, C. D.; Neurock, M. First Principles Analysis of the Electrocatalytic Oxidation of Methanol and Carbon Monoxide. *Top Catal* **2007**, *46*, 306–319.

(19) Neurock, M.; Janik, M. J.; Wieckowski, A. A First Principles Comparison of the Mechanism and Site Requirements for the Electrocatalytic Oxidation of Methanol and Formic Acid Over Pt. *Faraday Discuss* **2009**, *140*, 363–378.

(20) Ormerod, R. M.; Baddeley, C. J.; Hardacre, C.; Lambert, R. M. Chemisorption and Reactivity of Furan on Pd(111). *Surf. Sci.* **1996**, *360*, 1–9.

(21) Caldwell, T. E.; Abdelrehim, I. M.; Land, D. P. Furan Decomposes on Pd(111) at 300 K To Form H and CO plus C3H3, Which Can Dimerize to Benzene at 350 K. *J. Am. Chem. Soc.* **1996**, *118*, 907–908.

(22) Bradley, M. K.; Robinson, J.; Woodruff, D. P. Surface Science The Structure and Bonding of Furan on Pd (111). *SUSC* **2010**, *604*, 920–925.

(23) Pang, S. H.; Medlin, J. W. Adsorption and Reaction of Furfural and Furfuryl Alcohol on Pd(111): Unique Reaction Pathways for Multifunctional Reagents. *ACS Catal.* **2011**, *1*, 1272–1283.

(24) Mark, L. O.; Jenkins, A. H.; Heinz, H.; Medlin, J. W. Furfuryl Alcohol Deoxygenation, Decarbonylation, and Ring-Opening on Pt. *Surf. Sci.* **2018**, *677*, 333–340.

(25) Endo, M.; Matsumoto, T.; Kubota, J.; Domen, K.; Hirose, C. Formation of Formate in the Deep Oxidation of Methanol on Pt(111) under UHV Condition Studied by IRAS. *J. Phys. Chem. B* **2000**, *104*, 4916–4922.

(26) Crew, W. W.; Madix, R. J. Oxidative Coupling and Ring Opening of Furan on Ag(110): Formation of Maleic Anhydride, Benzene, and Bifuran. *J. Am. Chem. Soc.* **1993**, *115*, 729–736.

(27) Pourbaix, M.; Franklin, J. *Atlas of Electrochemical Equilibria in Aqueous Solution*; Pergamon, 1966.

(28) Kwon, Y.; Schouten, K. J. P.; Koper, M. T. M. Mechanism of the Catalytic Oxidation of Glycerol on Polycrystalline Gold and Platinum Electrodes. *ChemCatChem* **2011**, *3*, 1176–

1185.

(29) Cuesta, A.; Cabello, G.; Osawa, M.; Gutie, C. Mechanism of the Electrocatalytic Oxidation of Formic Acid on Metals. *ACS Catal*. **2012**, *2*, 728–738.

(30) Verdeguer, P.; Merat, N.; Gaset, A. Lead / Platinum on Charcoal as Catalyst for Oxidation of Furfural. Effect of Main Parameters. *Appl*. *Catal*. *A Gen*. **1994**, *112*, 1–11.

(31) Bhogeswararao, S.; Srinivas, D. Catalytic Conversion of Furfural to Industrial Chemicals over Supported Pt and Pd Catalysts. *J*. *Catal*. **2015**, *327*, 65–77.

(32) Guo, X.; Yates, J. T. Dependence of Effective Desorption Kinetic Parameters on Surface Coverage and Adsorption Temperature: CO on Pd(111). *J*. *Chem*. *Phys*. **1989**, *90*, 6761–6766.

(33) Kershner, D. C.; Medlin, J. W. Adsorption and Reaction of SiH4 and Oxygen on Pd(111). *Surf*. *Sci*. **2008**, *602*, 786–794.

(34) Kresse, G.; Furthmüller, J. Efficient Iterative Schemes for Ab Initio Total-Energy Calculations Using a Plane-Wave Basis Set. *Phys*. *Rev*. *B* **1996**, *54*, 11169–11186.

(35) Blöchl, P. E. Projector Augmented-Wave Method. *Phys*. *Rev*. *B* **1994**, *50*, 17953–17979.

(36) Perdew, J. P.; Chevary, J. A.; Vosko, S. H.; Jackson, K. A.; Pederson, M. R.; Singh, D. J.; Fiolhais, C. Atoms, Molecules, Solids, and Surfaces: Applications of the Generalized Gradient Approximation for Exchange and Correlation. *Phys*. *Rev*. *B* **1992**, *46*, 6671–6687.

(37) Giannozzi, P.; Baroni, S. Vibrational and Dielectric Properties of C60 from Density-functional Perturbation Theory. *J*. *Chem*. *Phys*. **1994**, *100*, 8537–8539.

(38) Matsushita, T. Dissociation of Oxygen Admolecules on Rh(111), Pt(111), and Pd(111) Surfaces at Low Temperatures. *Surf. Sci.* **1985**, *157*, 297–318.

(39) Parker, D. H.; Koel, B. E. Chemisorption of High Coverages of Atomic Oxygen on the Pt(111), Pd(111), and Au(111) Surfaces. *J. Vac. Sci. Technol* **1993**, *8*, 2585–2590.

(40) Allers, K. H.; Pfnür, H.; Feulner, P.; Menzel, D. Fast Reaction Products from the Oxidation of CO on Pt(111): Angular and Velocity Distributions of the CO2 product Molecules. *J. Chem. Phys.* **1994**, *100*, 3985–3998.

(41) Rico, M.; Barrachina, M.; Orza, J. M. Fundamental Vibrations of Furan and Deuterated Derivatives. *J. Mol. Spectrosc.* **1967**, *24*, 133–148.

(42) Fisher, G. B.; Gland, J. L. The Interaction of Water with the Pt(111) Surface. *JSurface Sci.* **1980**, *94*, 446–455.

(43) Horiuchi, C. M.; Israel, B. T.; Medlin, J. W. Adsorption and Reaction of 2(5H)-Furanone on Pt(111) and Pd(111): Divergent Ring-Opening Pathways of an Unsaturated Cyclic Ester. *J. Phys. Chem. C* **2009**, *113*, 14900–14907.

(44) Bent, B. E.; Mate, C. M.; Crowell, J. E.; Koel, B. E.; Somorjai, G. a. Bonding and Thermal Decomposition of Propylene, Propadiene, and Methylacetylene on the Rhodium(111) Single-Crystal Surface. *J. Phys. Chem.* **1987**, *91*, 1493–1502.

(45) Shi, D.; Vohs, J. M. Deoxygenation of Biomass-Derived Oxygenates: Reaction of Furfural on Zn-Modified Pt(111). *ACS Catal.* **2015**, *5*, 2177–2183.

(46) Lee, A. F.; Chang, Z.; Ellis, P.; Hackett, S. F. J.; Wilson, K. Selective Oxidation of Crotyl

Alcohol Over Pd(111). *J. Phys. Chem. C* **2007**, *111*, 18844–18847.

(47) Abon, M.; Bertolini, J. C.; Billy, J.; Massardier, J.; Tardy, B. Adsorption States of Benzene and Toluene on Pt(111): A Vibrational Eels, $\Delta\phi$, AES and TDS Study. *Surf. Sci. Lett.* **1985**, *162*, A594.

(48) Strandman-Long, L.; Murto, J. Furfuryl Alcohol—III. Infrared, Matrix Infrared and Raman Spectra and Ab Initio and Normal Coordinate Calculations. *Spectrochim. Acta Part A Mol. Spectrosc.* **1981**, *37*, 643–653.

(49) Davis, J. L.; Barteau, M. A. Spectroscopic Identification of Alkoxide, Aldehyde, and Acyl Intermediates in Alcohol Decomposition on Pd(111). *Surf. Sci.* **1990**, *235*, 235–248.

(50) Columbia, M. R.; Crabtree, A. M.; Thiel, P. A. The Temperature and Coverage Dependences of Adsorbed Formic Acid and Its Conversion to Formate on Pt(111). *J. Am. Chem. Soc.* **1992**, *114*, 1231–1237.

(51) Linic, S.; Jankowiak, J.; Barteau, M. A. Selectivity Driven Design of Bimetallic Ethylene Epoxidation Catalysts from First Principles. *J. Catal.* **2004**, *224*, 489–493.

(52) Gong, L.; Agrawal, N.; Roman, A.; Holewinski, A.; Janik, M. J. Density Functional Theory Study of Furfural Electrochemical Oxidation on the Pt (111) Surface. *J. Catal.* **2019**, *373*, 322–335.

(53) Roman, A. M.; Hasse, J. C.; Will Medlin, J.; Holewinski, A. Elucidating Acidic Electro-Oxidation Pathways of Furfural on Platinum. *ACS Catal.* **2019**, *9,* 10305-10316.

Table of Contents Figure

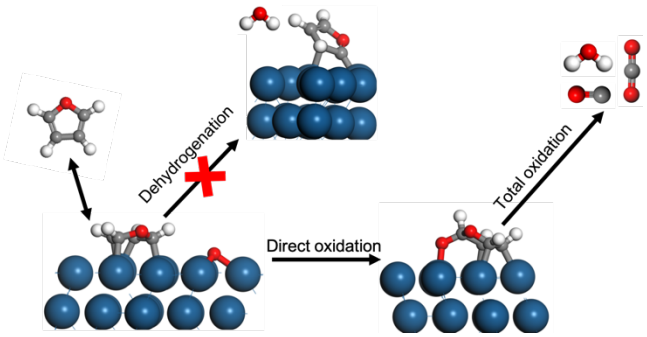
Dehydrogenation
Direct oxidation
Total oxidation